WAVE INTERACTIONS WITH A MULTITUDE OF FLOATING CYLINDERS

by Masashi KASHIWAGI

Research Institute for Applied Mechanics, Kyushu University
6-1 Kasuga-koen, Kasuga-city, Fukuoka 816-8580, Japan

1. Introduction

A column-supported type very large floating structure (VLFS), consisting of a thin upper deck and a multitude of buoyancy columns, is considered to be advantageous in that the wave forces and hence wave-induced responses are small relative to a box-shaped pontoon type. However, when a large number of identical bodies are placed in an array with equal separation distance, near-resonant modes may occur between adjacent bodies at some critical frequencies, and cause large wave forces on each element of the array.

In this paper, 64 truncated cylinders arranged in 4 rows and 16 columns are considered as a part of a real structure to check occurrence of near-resonant modes and performance of the wave interaction theory based on the potential flow. Experiments are conducted to measure the wave forces on a couple of element cylinders, as well as the total force on all cylinders, and the wave elevation along the longitudinal center line. Numerical computations are also performed using Kagemoto & Yue's interaction theory, with special care paid on the numerical accuracy and convergence.

Attention is focused on variation of the wave elevation and forces near critical frequencies. Since the reflection of waves is related closely to the steady drift force and moment, computations of the mean drift force and moment based on the momentum-conservation principle are implemented and compared with corresponding experiments.

2. Wave Interaction Theory

We consider a column-supported type VLFS, in which a great number of identical columns are placed in a rectangular array with equal separation distance. The elementary column considered here is a truncated circular cylinder with radius a and draft d. The distance between centerlines of adjacent cylinders is $2s$ in both x- and y-axes. The positive z-axis is directed downward, with $z = 0$ the undisturbed free surface and $z = h$ the constant water depth. Incident plane waves propagate in the direction with angle β relative to the positive x-axis.

The boundary conditions are linearized and the potential flow is assumed. Then, we express the velocity potential in the form

$$\Phi(x,y,z,t) = \mathrm{Re}\big[\,\phi(x,y,z)\,e^{i\omega t}\,\big]\,, \tag{1}$$

$$\phi = \frac{gA}{i\omega}\Big[\,\phi_I + \phi_S - K\sum_{k=1}^{\infty}\frac{X_k}{A}\big\{\,\phi_k + \varphi_k\,\big\}\,\Big]\,, \tag{2}$$

where g, A, ω and K are respectively the gravitational acceleration, the amplitude of an incident wave, the circular frequency, and the wavenumber given by ω^2/g.

ϕ_I is the incident-wave velocity potential expressed by

$$\phi_I = \frac{\cosh k_0(z-h)}{\cosh k_0 h}\, e^{-ik_0(x\cos\beta + y\sin\beta)}\,, \tag{3}$$

where k_0 is a solution of the wave dispersion relation, $k_0 \tanh k_0 h = K$.

ϕ_S in (2) represents the scattering potential. Let the number of floating bodies be denoted by N_B. Then the scattering potential due to the j-th body, ϕ_S^j, may be expressed in the form

$$\phi_S^j = \big\{A_S^j\big\}^T\big\{\psi_S^j\big\}\,, \tag{4}$$

where $\{A_S^j\}$ is the unknown coefficient vector, and $\{\psi_S^j\}$ is the vector comprised of the progreesive and evanescent wave components, which can be expressed as

$$\{\psi_S^j\} = \left\{ \begin{array}{l} Z_0(z)\, H_m^{(2)}(k_0 r_j)\, e^{-im\theta_j} \\ Z_n(z)\, K_m(k_n r_j)\, e^{-im\theta_j} \end{array} \right\}. \tag{5}$$

Here

$$Z_0(z) = \frac{\cosh k_0(z-h)}{\cosh k_0 h}, \quad Z_n(z) = \frac{\cos k_n(z-h)}{\cos k_n h}, \tag{6}$$

and k_n is the evanescent-mode wavenumbers satisfying $k_n \tan k_n h = -K$ ($n = 1, 2, \cdots$). The local cylindrical coordinate system (r_j, θ_j, z) has been used, with the origin placed at the center of the j-th body. The number of terms in the θ-direction, m, is taken as $0, \pm 1, \pm 2, \cdots$.

Using the wave interaction theory developed by Kagemoto & Yue, the unknown coefficient vector in (4) can be determined, with all effects of interactions with other bodies taken into account exactly in the framework of the potential theory.

In the radiation problem, X_k in (2) denotes the complex amplitude of the k-th mode of motion. In the definition of the mode, not only rigid-body motions but also a set of "generalized" modes to represent elastic deflections of a deck are assumed to be included. ϕ_k is the velocity potential due to the single-body oscillation with unit velocity in the k-th mode (without any interactions), and φ_k is the remaining part due to hydrodynamic interactions with other bodies.

By solving the boundary-value problem for a single body, ϕ_k may be explicitly given in the form

$$\phi_k^j = \{\mathcal{R}_k^j\}^T \{\psi_S^j\}, \tag{7}$$

where $\{\mathcal{R}_k^j\}$ is known and referred to as the vector of radiation characteristics.

The problem for φ_k is essentially the same as the scattering problem, and thus its solution is given by

$$\varphi_k^j = \{A_k^j\}^T \{\psi_S^j\}, \tag{8}$$

where $\{A_k^j\}$ is unknown but can be determined in exactly the same way as for the scattering problem.

Collecting all contributions due to the body disturbance, the velocity potential except for ϕ_I in brackets of (2) (let us denote this potential by ϕ_B) can be expressed as

$$\left. \begin{array}{l} \displaystyle \phi_B = \sum_{j=1}^{N_B} \{\mathcal{A}^j\}^T \{\psi_S^j\}, \\[4mm] \displaystyle \{\mathcal{A}^j\} = \{A_S^j\} - K \sum_{k=1}^{\infty} \frac{X_k}{A} \left(\{\mathcal{R}_k^j\} + \{A_k^j\} \right). \end{array} \right\} \tag{9}$$

Then using (9), the wave elevation at any point on the free surface ($z = 0$) can be computed by

$$\zeta(x, y) = A \left[\phi_I(x, y, 0) + \phi_B(x, y, 0) \right]. \tag{10}$$

3. Velocity Potential at Far Field

At a large distance from the structure, evanescent-wave components decay. Thus we may consider only the progressive waves in (9) expressed by the Hankel function.

In terms of the global coordinate system O-$r\theta z$, the Hankel function can be written by Graf's addition theorem in the form

$$H_m^{(2)}(k_0 r_j)\, e^{-im\theta_j} = \sum_{\ell=-\infty}^{\infty} J_{m-\ell}(k_0 L_{j0})\, e^{-i(m-\ell)\alpha_{j0}} \left\{ H_\ell^{(2)}(k_0 r)\, e^{-i\ell\theta} \right\}, \tag{11}$$

where L_{j0} and α_{j0} are the radial distance and azimuth angle of the origin of the global coordinate system when viewed from the center of the j-th body, and r must be larger than L_{j0} for (11) being valid.

Substituting the above relation into (9), the disturbance potential at far field can be written as

$$\phi_B = \sum_{\ell=-\infty}^{\infty} A_\ell \left\{ Z_0(z)\, H_\ell^{(2)}(k_0 r)\, e^{-i\ell\theta} \right\}, \tag{12}$$

where A_ℓ ($\ell = 0, \pm1, \pm2, \cdots$) denotes the components of the vector given by

$$\{\mathcal{A}\} = \sum_{j=1}^{N_B} [M_{j0}]^T \{\mathcal{A}^j\}. \tag{13}$$

Here, $[M_{j0}]$ is the matrix when writing (11) in a matrix form, and $\{\mathcal{A}^j\}$ is defined in (9).

The incident-wave potential, ϕ_I given by (3), can be also expressed in terms of the cylindrical coordinate system. Therefore the total velocity potential can be written as

$$\phi = \frac{gA}{i\omega} \sum_{\ell=-\infty}^{\infty} Z_0(z) \Big\{ \alpha_\ell J_\ell(k_0 r) + A_\ell H_\ell^{(2)}(k_0 r) \Big\} e^{-i\ell\theta}, \tag{14}$$

where α_ℓ is the coefficient explicitly given by $\alpha_\ell = \exp\{i\ell(\beta - \pi/2)\}$.

4. Wave Drift Force and Moment

Based on the conservation principle of linear and angular momentum, we can relate the mean drift force and moment on a structure to the far-field potential. In the present case, necessary integrations with respect to z and θ for a large value of r can be analytically performed in terms of (14). The details of derivation are omitted here, but using orthogonality relations in trigonometric functions and Wronskian formulae for Bessel functions, we can obtain the following results:

$$\overline{F}_x = -\frac{\rho g A^2}{2} \frac{k_0}{K} \frac{k_0^2}{K + h(k_0^2 - K^2)} \operatorname{Im} \sum_{\ell=-\infty}^{\infty} \Big[2A_\ell A_{\ell+1}^* + \alpha_\ell A_{\ell+1}^* + A_\ell \alpha_{\ell+1}^* \Big], \tag{15}$$

$$\overline{F}_y = -\frac{\rho g A^2}{2} \frac{k_0}{K} \frac{k_0^2}{K + h(k_0^2 - K^2)} \operatorname{Re} \sum_{\ell=-\infty}^{\infty} \Big[2A_\ell A_{\ell+1}^* + \alpha_\ell A_{\ell+1}^* + A_\ell \alpha_{\ell+1}^* \Big], \tag{16}$$

$$\overline{M}_z = -\rho g A^2 \frac{1}{K} \frac{k_0^2}{K + h(k_0^2 - K^2)} \operatorname{Re} \sum_{\ell=-\infty}^{\infty} \ell \Big[A_\ell A_\ell^* + \alpha_\ell A_\ell^* \Big]. \tag{17}$$

5. Experiments

A truncated circular cylinder with diameter $D\,(= 2a) = 114$ mm was used as an elementary float, and 64 cylinders were arranged in an array with 4 rows (in the y-axis) and 16 columns (in the x-axis) with equal separation distance of $2s = 2D$ between the centerlines of adjacent cylinders in both x- and y-axes. The draft of cylinders was set to $d = D$ and $2D$, but here the results of $d = 2D$ will be mainly shown.

Experiments were carried out in head waves with all motions fixed. Measured items were wave elevations at 16 points along the centerline of the array, wave forces on elementary cylinders placed at No. 1, No. 9, and No. 15 columns along No. 2 row, and at the same time the total forces on 64 cylinders. The frequency range in measurements was $Ks = 0.2 \sim 1.6$ and the wave steepness H/λ (the ratio of wave height to wave length) was set to approximately $1/50$.

6. Results and Discussion

After convergence of numerical results was checked for $Ks = 1.0$, $\beta = 0°$ and $h = 3d$, the number of terms in the θ-direction (M) and the number of evanescent modes (N) were determined to be $M = 4$ and $N = 3$, which yields an absolute accuracy of five decimals. In this case, the total unknowns for $N_B = 64$ are $(2M + 1) \times (N + 1) \times N_B = 2304$. To enhance numerical efficiency, the double symmetry relations with respect to the x- and y-axes are exploited, reducing the number of unknowns to $1/4$.

Although there are many measured results, only a couple of results are shown here, because of shortage of the space. Fig. 1 shows the wave elevation as a function of Ks, measured at between No. 1 and No. 2 columns (the upwave side). Likewise, Fig. 2 and Fig. 3 are the results near the midst of the array and the downwave side, respectively. We can see rapid variation at the upwave side and large-amplitude waves in the midst of the array for $Ks \simeq 0.8 \sim 1.24$. $Ks \simeq 1.24$ may correspond to the Neumann trapped mode, discussed by Maniar & Newman. Numerical results agree well qualitatively with experiments, but tend to overpredict as the point compared goes downstream. No breaking waves were observed in the experiments.

Thus the difference from the potential-theory results may be attributed to a decaying mechanism due to development of the oscillatory boundary layer or other viscous effects.

Figure 4 shows the surge drift force in head waves. Analogous to the wave elevation at the upwave side, rapid variation can be seen at frequencies less than $Ks \simeq 1.24$. When Ks is greater than this critical value, the waves are mostly reflected and thus the drift force becomes large. Although measured values are scattered, the overall agreement is favorable between computed and measured results.
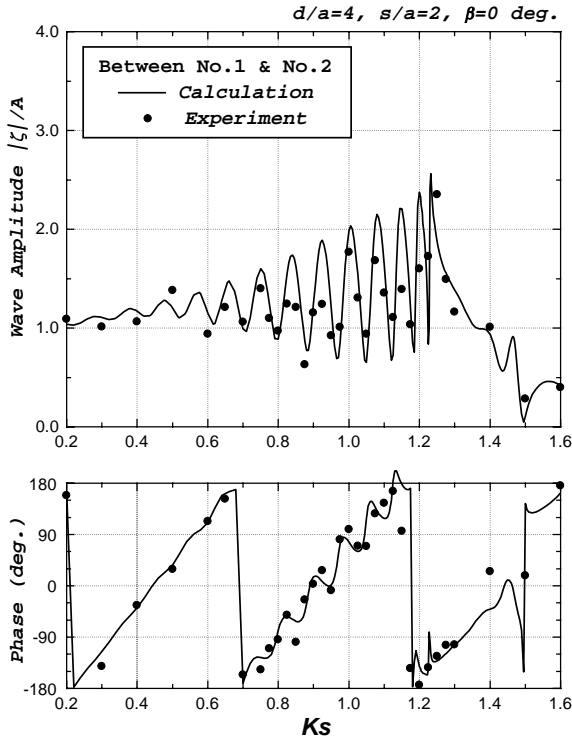
Fig. 1 Wave elevation at upwave side
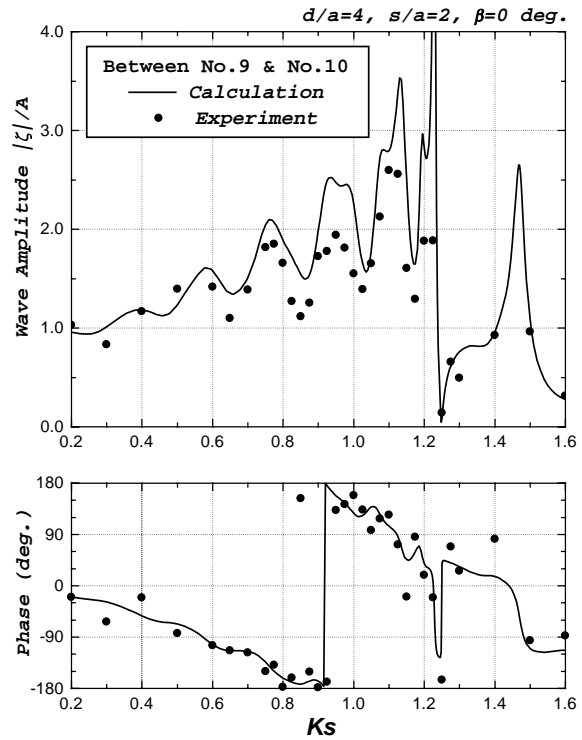
Fig. 2 Wave elevation at midst of the array
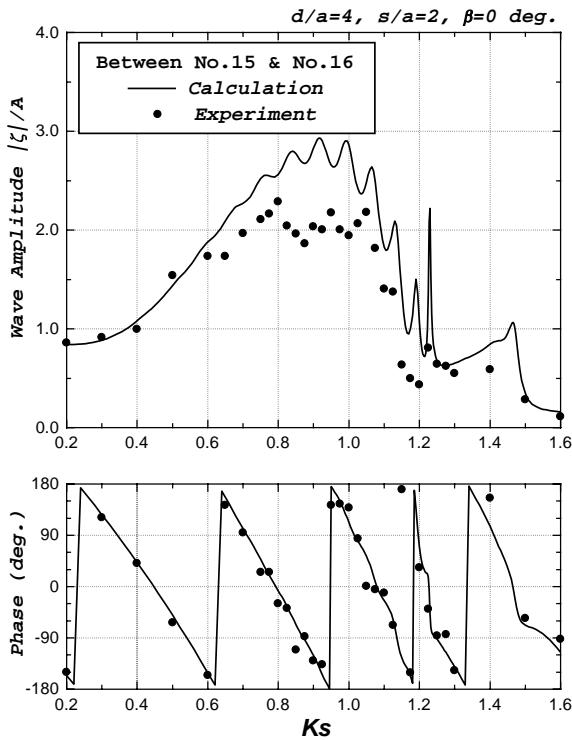
Fig. 3 Wave elevation at downwave side
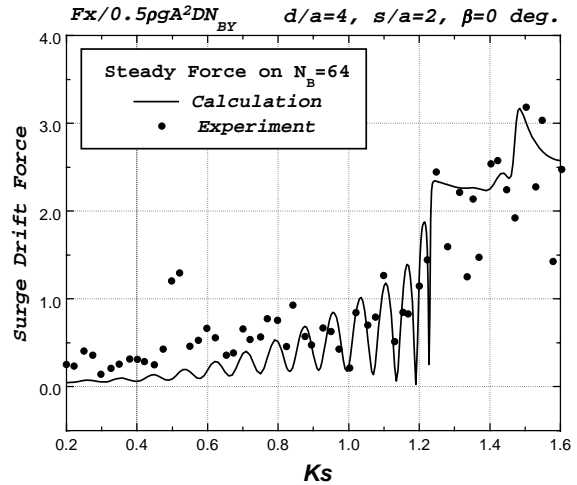
Fig. 4   Surge drift force acting on 64 cylinders arranged in 4 rows and 16 columns in head waves